Critical Dimension measurement: from synchrotron small angle X-ray scattering to industrial Optical Scatterometry techniques

Timothée Choisnet, Abdelali Hammouti, Vincent Gagneur, Jerome Reche, Guido Rademaker, Guillaume Freychet, Guillaume Jullien, Julien Ducote, Patrice Gergaud, Delphine Le Cunff

PROCEEDINGS OF SPIE

SPIEDigitalLibrary.org/conference-proceedings-of-spie

Critical dimension measurement: from synchrotron small angle x-ray scattering to industrial optical scatterometry techniques

Timothée Choisnet, Abdelali Hammouti, Vincent Gagneur, Jérôme Reche, Guido Rademaker, et al.

Timothée Choisnet, Abdelali Hammouti, Vincent Gagneur, Jérôme Reche, Guido Rademaker, Guillaume Freychet, Guillaume Jullien, Julien Ducote, Patrice Gergaud, Delphine Le Cunff, "Critical dimension measurement: from synchrotron small angle x-ray scattering to industrial optical scatterometry techniques," Proc. SPIE 12496, Metrology, Inspection, and Process Control XXXVII, 124961K (27 April 2023); doi: 10.1117/12.2657661

SPIE.

Event: SPIE Advanced Lithography + Patterning, 2023, San Jose, California, United States

Critical dimension measurement: from synchrotron Small Angle X-ray Scattering to industrial Optical Scatterometry techniques

Timothée Choisnet[a,b], Abdelali Hammouti[a,b], Vincent Gagneur[a,b], Jérôme Reche[b], Guido Rademaker[b], Guillaume Freychet[b,c], Guillaume Jullien[b], Julien Ducote[a], Patrice Gergaud[b] and Delphine Le Cunff[a].

[a] STMicroelectronics, 850 rue Jean Monnet, 38926 Crolles, France;
[b] Université Grenoble Alpes, CEA, Leti, F-38000 Grenoble, France;
[c] National Synchrotron Light Source-II, Brookhaven National Laboratory, Upton, New York 11973, United States

ABSTRACT

Critical Dimension (CD) control is essential in the semiconductor industry and becomes more challenging as photolithography limits keep getting pushed to reach technological nodes smaller than 10 nm. To ensure quality and control of the processes, it becomes necessary to explore new metrology techniques. In this sense, Critical Dimension Small-Angle X-ray Scattering (CDSAXS) has been identified as a potential candidate to determine the average shape of a line grating with a sub-nanometric precision. In this paper we benchmark the CDSAXS results to Optical Critical Dimension (OCD), Critical Dimension Scanning Electron Microscopy (CDSEM) and Transmission Electron Microscopy (TEM) measurements previously collected from industrial metrology tools at manufacturing line and in characterization laboratory. Emphasis is placed on the model used for CDSAXS and how to improve it. We discuss the differences between all these multi-scale and multi-physics techniques, and question our capacity to compare them.

Keywords: CD, CDSAXS, metrology, benchmark, OCD, SEM, TEM.

1. INTRODUCTION

The evolution of microelectronics and the reduction of component dimensions lead to new technological challenges, whether in terms of component design, integration or choice of materials. Metrological techniques used to control the properties of components, their dimensions and the correct behavior of fabrication processes are no exceptions to these challenges and capabilities limits are reached [1], [2].

Most used techniques based on direct imaging are SEM and TEM. They both use electron beams to probe the samples, respectively by scanning its surface and by transmitting the beam through it [1], [3], [4]. Another standard is OCD, an optical technique that reconstructs the profile of a periodic pattern based on its optical diffraction response with a lateral resolution of a few nanometers. As OCD is an indirect reconstruction technique, mathematical models are needed to refine the structural parameters that describe the structures [5]–[8]. The measurement spot averages over a surface of several hundreds of μm^2, making it well adapted for CD, pitch, height or even side-wall angle (SWA) measurements, but making it barely sensitive to process induced defectivity and local variations such as line roughness or pitch-walk [9]. On the other hand, SEM and TEM are suitable for such local variation detection, but their small fields of view (FoV) do not produce sufficient sampling with a single measurement.

Some techniques emerge, such as CDSAXS, which shows good potential. This technique has been developed for the past few years and has been demonstrated to be efficient for the reconstruction patterns with sub-nanometric resolution [10]–[13]. Sunday *et al*. expanded the approach with improving the reliability of the in-depth profile extraction with a more robust minimization algorithm, the creation of more complex model and spreading the measurements to wider material diversity [13], [14]. They also migrated the measurements from synchrotron to laboratory equipment with the use of a high flux and high energy lab source [15]. Reche *et al*. extended the approach to measure and extract the line edge roughness

Metrology, Inspection, and Process Control XXXVII, edited by John C. Robinson, Matthew J. Sendelbach, Proc. of SPIE Vol. 12496, 124961K
© 2023 SPIE · 0277-786X · doi: 10.1117/12.2657661

[16], [17]. This technique, often presented as a reference technique in terms of resolution, is however still very rarely implemented in microelectronics clean rooms. Measurement times remain long and data processing complex. However, its high resolution and large field of view makes the CDSAXS a good candidate to calibrate other metrology techniques more compatible with the constraints of industrial production.

In this study, benchmarking of these different techniques is done on same samples in the aim of developing a reference standard for CD measurement with ST Microelectronics' OCD tools. We aim to improve the measurements by comparing different metrology tools and combining their respective strengths.

The measured samples are first presented. Their dimensions and characteristics must be adapted to all of our techniques, whose specifications and parameters are introduced. We then present, compare and comment the results obtained for pitch and CD extraction with all techniques. While significant differences can be observed from technique to technique, we report that a direct comparison is limited by the difference in the modeling approach of each technique.

2. METHODS

We first designed samples compatible with the different techniques considered. The first constraint is the FoV, designating the probed area for each technique. It varies from 500 µm × 25 µm for CDSAXS to 1.35 µm × 1.35 µm for CDSEM, and even 100 nm × 100 nm at maximum magnification for TEM. The second constraint is the pitch. In order to be in the range where all the techniques are performant, the pitch needs to be set below few hundreds nanometers to match CDSAXS requirements and above few dozens of nanometers to match the OCD resolution, 190 nm being the lowest wavelength accessible on our tool.

Taking into account the previous experimental constraints, the samples processed in CEA Leti's clean room contain multiple 1.5 mm × 1 mm measurement targets within each 26 mm × 33 mm lithographic field. They present a constant pitch of 112 nm, measurable with all techniques.

2.1 Sample specification and description

Simple silicon-based line gratings are used in order to simplify the comparisons between techniques and the models definitions. The samples have followed steps of 193 nm immersive lithography and dry etching (Figure 1a, b). To passivate the surfaces and prevent evolution over time, the gratings were coated with a conformal oxide with an estimated thickness around 1.4 nm. An exposure matrix (EM) introduced during the lithographic process allows us to have a wide nominal range of measurable CDs. This study is focused on three fields of interest: (0, -3), (0, 0) and (0, 5) (Figure 1a, b) with respective aimed CD values of 36 nm, 50 nm and 60 nm.

The obtained structures observed by TEM (Figure 1d) are not perfect straight lines but rather rounded trapezoids. The white area covering the sample is due to the SiO_2 passivation.

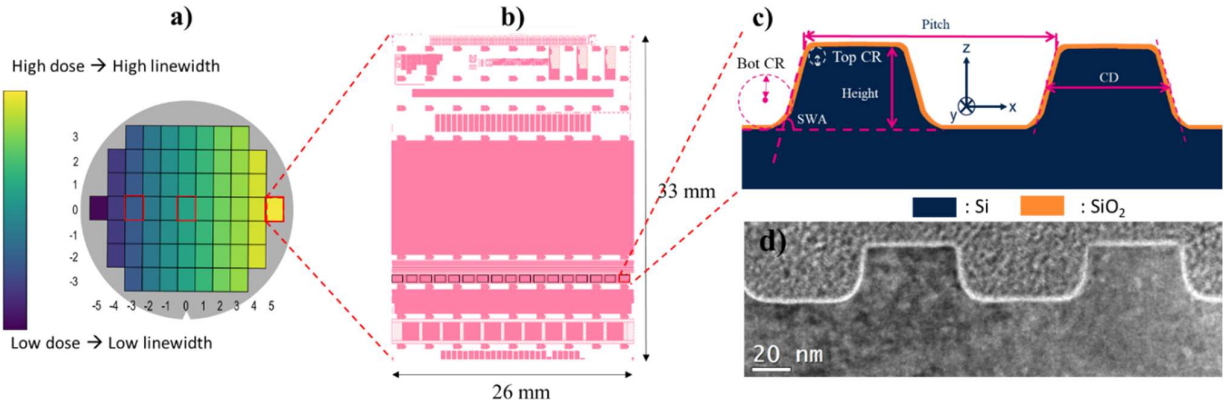

Figure 1. Presentation of a) our wafer with the exposure map, b) the mask for each lithographic field, c) the representation and parametrization of our structures within the measurement boxes and d) an actual TEM image of our structures.

2.2 Workflow and measurement techniques

Several sister wafers were processed simultaneously. As 300 mm wafers are not measurable on the synchrotron beamline nor on TEM laboratory tool, we had to manage our workflow. CDSEM and OCD characterizations were first performed on all of our sister wafers in the clean room environment. One of them was then cleaved to be measured with CDSAXS and TEM. The processing of multiple sister wafers allowed us to perform destructive measurements and still have remaining wafers to be used as certificates.

CDSAXS experiments were performed at the Soft Matter Interfaces Beamline (SMI, Beamline 12-ID) at the National Synchrotron Light Source (NSLS) II with a photon energy of 16.1 keV to enable a 30% transmission of the X-rays through the 700-µm thick silicon wafer. Scattered intensity is recorded with Pilatus3 1M which is positioned at 8.29 meters from the sample. With a rotation φ between -60 ° and 60 ° with a step of 1 ° along the y-axis (Figure 2b), a cartography of the reciprocal space (q_y, q_z) was obtained and shown on Figure 4c. This cartography gives information on the (xz) plan, enabling 3D reconstruction of the in-depth line profile. The intensity modulations observed along the Bragg rods (horizontal brighter lines) are extracted. The extracted experimental intensity profiles are used as input in a minimization process in order to find the best simulated profile. Here we decide to describe the line profile as a stack of trapezoids and a comparison between the simulated and experimental data is plotted on Figure 4c.

The Full Width Half Maximum (FWHM) of the X-ray beam is 250 µm × 25 µm (HxV) at the sample position, and extends to 500 µm × 25 µm at maximum φ = ± 60 ° rotation. Because this FoV is the largest amongst all the techniques in this study, we must adapt the measurements. This adaptation, displayed in Figure 2a, involves measuring multiple points within the SAXS FoV and averaging the results with a Gaussian weight that matches this SAXS spot.

Few TEM lab measurements were done on a 200 kV Tecnai from Thermofisher on the same cleaved sample measured by SAXS. FoV of 100 nm × 100 nm, 110 nm × 110 nm and 130 nm × 130 nm were obtained, respectively for fields (0, -3), (0, 0) and (0, 5). The electron source is a FEG (Field Emission Gun), and our images (Figure 1d) were acquired in bright field. 15 images were taken over the SAXS spot for statistic enhancement.

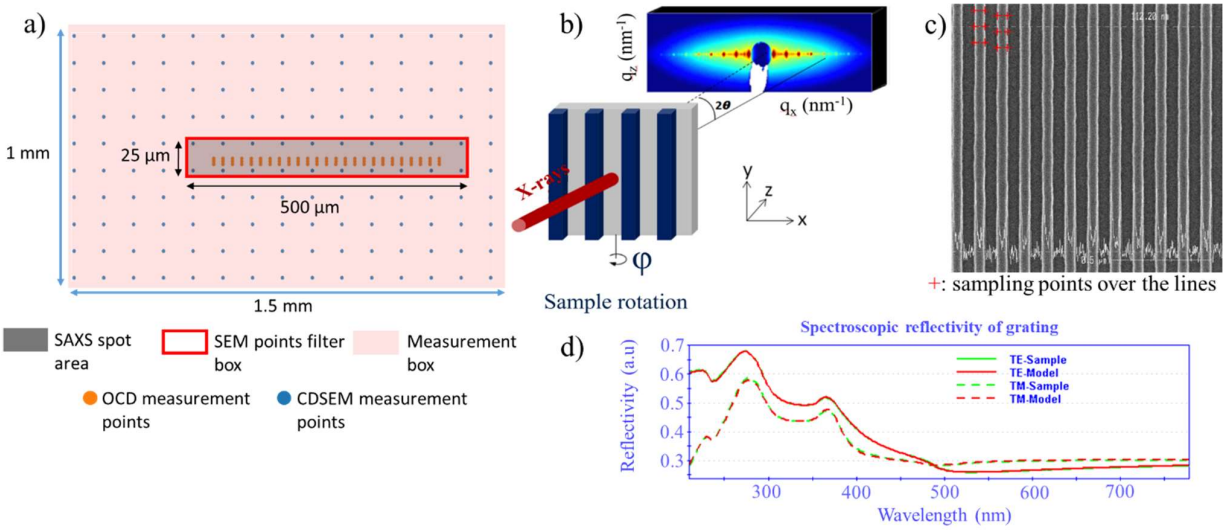

Figure 2. a) Comparison of key sizes and description of the measurement zones for SEM, OCD and SAXS (not at scale), b) SAXS transmission measurement geometry [18], c) SEM image and d) OCD spectrum.

For SEM measurements, we used the equipment CG5000 from HITACHI in ST Microelectronics Crolle's clean room, with an electron accelerating voltage of 800 eV and a probe current of 8 pA. The 1.35 µm × 1.35 µm FoV allows CDs and pitches averaging on maximum 11 structures, with 200 points along each line and a pixel size of 1.32 nm × 1.32 nm. The CDSEM top-view geometry makes it slightly different from the other techniques that measure in depth regions. The measurements are made between 80% maxima of the grey levels signal, inducing an offset between the CDSEM measured

CD and the CD taken at mid height as we define it. CD and pitch are measured 150 times each on the whole surface of the box, as shown on Figure 2a, before being filtered.

OCD acquisitions were performed on ATLAS XP+ and ATLAS 2 equipment from ONTO Innovations. These tools allow optic ranges of 190 nm - 1000 nm, and average structures over a 50 µm × 50 µm spot. Acquisitions are a combination of ellipsometry and reflectometry. Unlike CDSEM, we directly performed the 75 OCD acquisitions within the SAXS spot.

3. RESULTS

3.1 Pitch extraction

The pitch p is fixed to its nominal value of 112 nm in our OCD model and is thus not measured. Moreover, TEM is too sensitive to roughness, making pitch measurements with this technique irrelevant. That is why p was only measured with CDSEM and CDSAXS. The SEM pitch measurement conditions are the same as for the CD. However, no repeatability measurements were performed for the pitch; we thus rely on the ST's monitoring pitch measurements on a calibration wafer presenting similar silicon-etched line gratings. The resulting 3σ variation is 0.1 nm. Results are displayed in the Table 1.

For the CD-SAXS, the pitch can be extracted from the position of the Bragg rods on the 2D image collected at $\varphi = 0°$ and shown on Figure 2b. The Bragg peak positions in q_x after a 1D integration at $q_z = 0$ nm^{-1} enable the extraction of p: by combining the definition of the $\vec{q}$ vector and Bragg's law we obtain the relation 3.1 between p and the slope of the peaks' position as a function of their order. The extraction process is displayed on Figure 3a.

$$p = \frac{2\pi}{\partial q_{x,n}/\partial n} \tag{3.1}$$

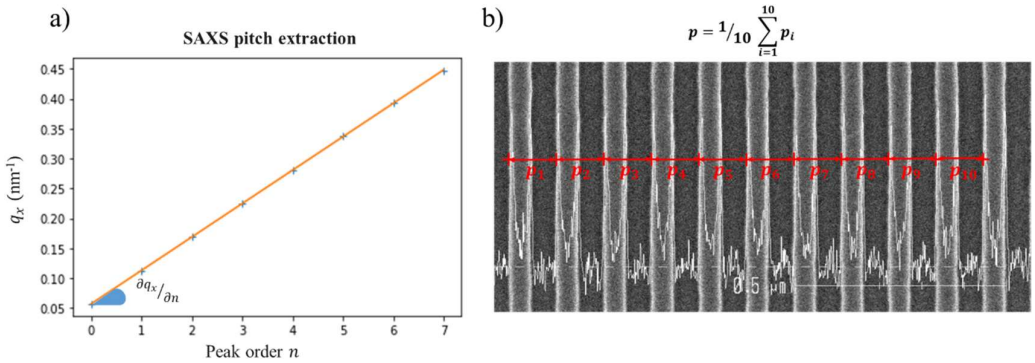

Figure 3. Pitch extraction with a) CDSAXS and b) CDSEM.

We can then express p using experimental parameters:

$$p = n\lambda\frac{R}{x_n} \tag{3.2}$$

And define the error propagation of the pitch calculation as:

$$\Delta p = p \times \sqrt{\left(\frac{\Delta\lambda}{\lambda}\right)^2 + \left(\frac{\Delta x_n}{x_n}\right)^2 + \left(\frac{\Delta R}{R}\right)^2} \tag{3.3}$$

Where $\lambda = 7.7009 \times 10^{-2}$ nm ± 0.0008×10^{-2} nm is the wavelength of the incident beam, $x_n = 5700.0$ µm ± 8.6 µm the position of the n peak and $R = 8.290$ m ± 0.002 m the sample-to-detector distance [19]. Knowing these parameters and their uncertainties we obtained an uncertainty for pitch $\Delta p = 0.2$ nm.

Table 1. Summary table for pitch measurements with CDSAXS and CDSEM. The uncertainty for CDSAXS is the calculated analytic uncertainty, while it is 3σ of repeatability measurement on a calibration wafer for CDSEM.

Average measured pitch (nm) (target = 112 nm)		Lithographic field		
		(0, -3)	(0, 0)	(0, 5)
Technique	CDSAXS	112.1 ± 0.2	112.0 ± 0.2	112.0 ± 0.2
	CDSEM	112.1 ± 0.1	112.1 ± 0.1	112.1 ± 0.1

SAXS and CDSEM present respective uncertainties of 0.2 nm and 0.1 nm. These ranges are not calculated in the same way: they include an analytical error spread and a repeatability dispersion of 3σ on a calibration wafer. Comparing them as is is not ideal, and it would be better if they were both evaluated identically. We can however see that these techniques have a good agreement and yield results that are close to the nominal 112 nm value, and this for the 3 fields of interest.

3.2 CD measurements

The OCD model defined from TEM images and the fitted spectrum are displayed on Figure 4a, b. The model presents a stack of three trapezoids: two for the rounded regions and one for the body of the line. It has three floating parameters (Figure 1c): the height, the SWA of the central trapeze and the bottom CD. The pitch, the oxide thickness and the corner roundings (CR) are fixed to namely 112 nm, 1.4 nm, 3 nm (top CR) and 10 nm (bot CR).

In SAXS, the reconstruction of the parameters of the line relies on the relative intensity variations of the scattering peaks, and requires modelling and fitting as for OCD. The model we evaluate in this study consists of a stack of N constant-height trapezoids. It presents $2+N$ floating parameters: the total height, the bottom CD and one SWA for each trapeze. Our studies showed that the optimum is reached for $N = 6$ trapezoids, as shown on Figure 4d, leading to eight floating parameters. SAXS measurements were reproduced only a few times for each field, from 2 for the field (0, 5) to 8 for the field (0, 0). Since it is too low for a relevant statistic information, we only evaluated the dispersion with the max-min range on the obtained CD values.

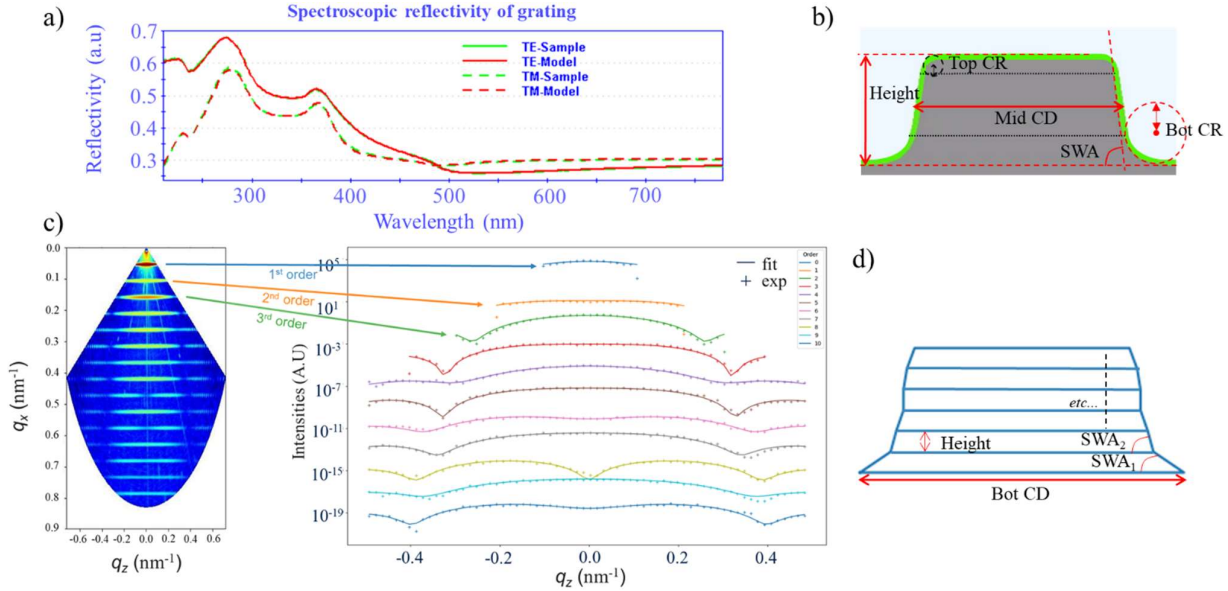

Figure 4. Numerical inverse problem resolution for a) OCD and c) CDSAXS (intensities are arbitrarily offset for visualization). We also show the resulting reconstructed line for both techniques: b) OCD and d) CDSAXS.

The CDs were measured with all four techniques and the results are compared in the Figure 5. The uncertainties for OCD and CDSEM are calculated with the 3σ distribution of the repeatability measurements, consisting in respectively 30 and 10 measurements in the center of the box. TEM uncertainty has been evaluated at 5% by considering the reference standard and the highly operator-dependent imaging and measurement.

CDSEM measurement and filtering within the SAXS spot delimitation give average CDs of 37.7 nm ± 0.1 nm, 49.1 nm ± 0.2 nm and 59.1 ± 0.1 nm respectively for fields (0, -3), (0, 0) and (0, 5). The dispersion remains around the Angstrom for all fields, and is mainly due to inhomogeneity and line roughness.

OCD yields CDs of 39.1 ± 0.1 nm, 50.3 ± 0.1 nm and 60.7 nm ± 0.1 nm respectively. The constant 3σ dispersion on the repeatability measurement of 0.1 nm confirms that OCD is highly precise.

We obtain respective estimations of 37.5 nm ± 0.1 nm, 49.4 ± 0.6 nm and 58.6 nm for the middle CD with this 6-trapezoid SAXS model. Note that for the field (0, 5) the 2 measurements yield the same CD, making the max-min range equal to zero as we can see on Figure 5. We also started to evaluate a second model with a rounded trapezoid. This second models aims to mimic TEM images and the OCD model more accurately in order to improve the reconstruction and enable a more accurate OCD/CDSAXS comparison. The rounding model presents five floating parameters: top CD, height, SWA of the trapeze's body and top and bot CRs. It yields CDs of 38.3 nm ± 0.1 nm, 50.2 ± 0.4 nm and 59.5 nm respectively. Further investigations are needed, and this model will be more deeply studied more in a future publication.

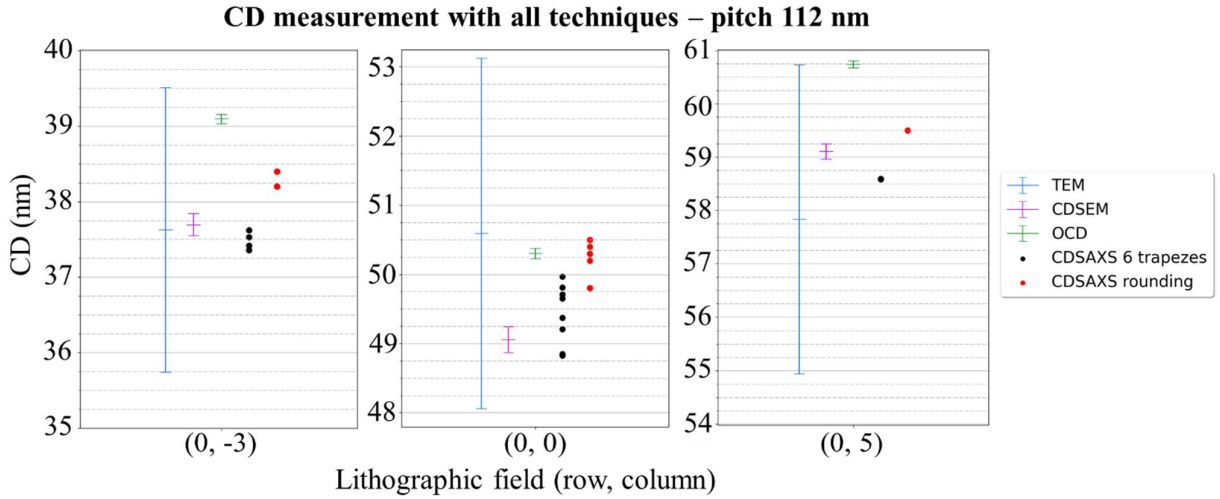

CD measurements (nm)		Technique				
		CDSEM (CD ± 3σ repeatability)	OCD (Mid CD ± 3σ repeatability)	CDSAXS 6 trapezes (Mid CD ± 0.5 * (max-min))	CDSAXS rounding (Mid CD ± 0.5 * (max-min))	TEM (± 5%)
Field	(0, -3)	37.7 ± 0.1	39.1 ± 0.1	37.5 ± 0.1	38.3 ± 0.1	37.6 ± 1.9
	(0, 0)	49.1 ± 0.2	50.3 ± 0.1	49.4 ± 0.6	50.2 ± 0.4	50.6 ± 2.5
	(0, 5)	59.1 ± 0.1	60.7 ± 0.1	58.6	59.5	57.8 ± 2.9

Figure 5. Results of our CD measurements and their uncertainties for pitch 112 nm line for three fields of interest.

Finally, the TEM measurements give respective average mid CDs of 37.6 nm ± 1.9 nm, 50.6 nm ± 2.5 nm and 57.8 nm ± 2.9 nm.

3.3 CDSEM and OCD correlation

The large range of CDs obtained with the exposure matrix allowed us to evaluate the correlation between CDSEM and OCD by plotting the values for the four fields of interest (Figure 6). The 0.994 slope shows that the correlation is good between these techniques. We also obtain a y-intercept of 1.6 nm.

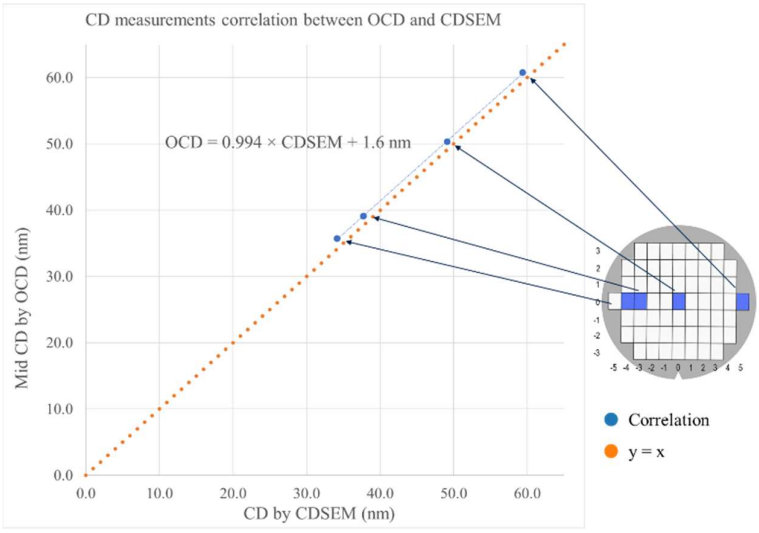

Figure 6. Correlation between SEM and OCD measurements. CDs are taken at the four interest fields (0, -4), (0, -3), (0, 0) and (0, 5).

4. DISCUSSION

4.1 CD analysis

As expected, TEM measurements are too local and thus sensitive to line edge roughness along the *y*-axis (Figure 1d) to be quantitatively relevant: the image only integrates over the 100 nm thickness of the lamella along this axis, and each line is different from another. The 5% range of uncertainty, yielding 1.9 nm, 2.5 nm and 2.9 nm for the different lithographic fields, is very high in comparison with that of the other techniques that go up to 0.6 nm for CDSAXS 6-trapezoid model and down to 0.1 nm for OCD. The interest of TEM measurements remains in the quality of the images that allow accurate models definition.

While the SEM measurements are also very local, the averaging of 200 points along each line makes the acquisitions less sensitive to line roughness, increasing the technique's precision. The CD obtained is however lower than the other techniques, mainly due to the difference in the location where the CD is measured. While all the reported values are the mid-CD ones, the SEM only detects the 80% signal-height CD. However, CDSEM and OCD present comparable very low dispersions, which is expected since these are the actual conventional techniques for CD control.

As for CDSAXS, the 6-trapezoids model does not overlap with OCD in spite of the good agreement between them. It is to be expected when comparing two model-dependent techniques treated separately: the numerical processes are not identical and the models are different because they are not created on a single software or script. It would be optimal to create one single script of our own to treat all the raw data from the different techniques with a single model we would define.

In our SAXS treatment, the approximation has been made that SiO_2 and Si had the same electronic densities (namely 0.67 e^-/A^3 and 0.71 e^-/A^3) to simplify the simulations. SAXS sensitivity residing in the electronic density contrasts, this approximation must be suppressed to increase the results accuracy. This differentiation is also essential if we want to extend our work to more complex structures with multiple materials, more representative of actual technologies. Lastly, the 6 trapezoid model seems to give lower results than it should because of "inflexions" at mid height of the trapezes during reconstruction (see Figure 4d). This is systematic in this model, and could be due to parameters correlation causing the algorithm to diverge because of the high number of floating parameters. This issue could be resolved by reducing the number of floating parameters, having a more accurate model or by adding "regularization" on the code, i.e putting penalties to the fit quality evaluation as the algorithm iterates when the SWAs lead to such profiles. By defining the rounded trapezoid model, we aim to have such a "more accurate" model. In this model, which is to be submitted in a next paper, the trapeze is separated in three regions: the two rounded regions, defined with circles, and the body of the trapeze which consists in one whole trapeze. Instead of having constant-height trapezes for rounded regions and the trapeze body, we concentrate the resolution on the CRs. This approaches not only the actual structures seen on TEM images, but also the

OCD model. The reduction of the number of floating parameters from eight to five reduces the inter-parameters correlation (as discussed just above) and could resolve the "inflexion" issue.

Along the improvement of the model, further SAXS studies are needed to properly evaluate the uncertainty induced by the modelling process. This could be done with a Monte Carlo Markov Chain (MCMC) algorithm for the fitting process, or by extracting covariance matrixes. Such accuracy determination is of high necessity in order to determine SAXS ability to be a reference technique. It would also allow us to homogenize the uncertainty evaluations of all our techniques, and make more relevant comparisons. To evaluate the technique's precision, a more convenient experimental setup is needed: synchrotron setup does not allow large statistical measurements such as repeatability or reproducibility. The main constraints for laboratory transmission SAXS are the need of a high-flux and high energy X-ray source to prevent the absorption from silicon subtrates. Laboratory tools are emerging, but the flux sources remain too inefficient for SAXS measurements and synchrotron-based measurements remain the top choice [15]. This lack of statistics and knowledge on the modelling-induced errors gives results that are not reliable, especially for the field (0, 5) where we only have two measurements that give the same values.

4.2 CDSEM and OCD correlation

We can note that the correlation between OCD and CDSEM is very good, with a 0.994 slope. We can however wonder were the 1.6 nm y-intercept originates from. It is tempting to assume that the measurements at 80% of signal height correspond to measurements at 80% of the line height. We could thus try to calculate the offset between CDs at 50% and 80% of the line and see if this matches the y-intercept, but we can't for multiple reasons. The two main ones are, as illustrated on Figure 7, the variation of collected electrons around the edges of the trapeze (Figure 7a) and dispersion of the e-beam spot that induces an error on the signal width (Figure 7b). Therefore, a constant bias will always be present on the measurements, invalidating the 80% signal / 80% height assumption. However, the two edges of the trapeze being distant of approximately 40 nm, we can assume that they are independent. This explains why CDSEM is highly precise and correlates well with OCD.

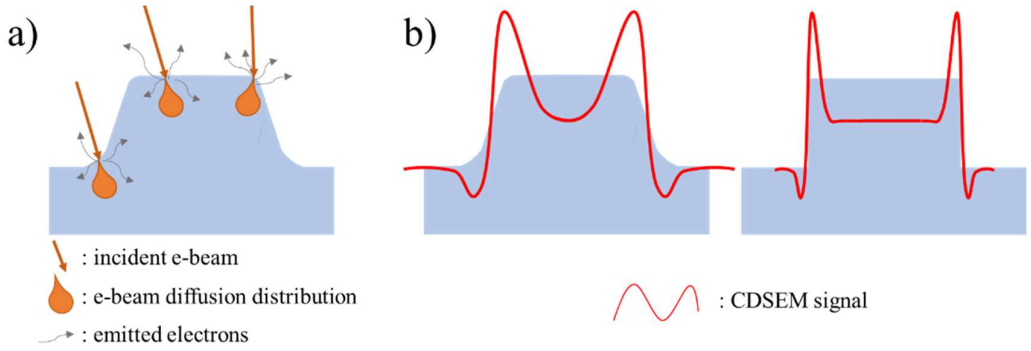

Figure 7. Illustration of the main limitations of CDSEM accuracy: a) shows the signal variations on the edges of the trapeze and b) illustrates the non-zero width of the signal even for a 90 ° SWA.

Errors can also originate from the OCD model, which can be improved by deepening the studies on its parameters (their ranges of variation, nature, definitions etc.) The use of an existing software makes this model-development phase easier than with CDSAXS. We could for example try to make the corner roundings floating parameters and see how the resulting mean square error (MSE) varies.

5. CONCLUSION AND PERSPECTIVES

In this study OCD, CDSEM, TEM and CDSAXS were benchmarked. Comparing multi-scale techniques that use different physical principles in various environments (clean room, synchrotron and characterization lab) proved to be challenging in terms of logistics and data treatment. Significant differences of the CD were found dependent on the measurement technique. The TEM measurements are key to build the model for the indirect techniques such as OCD and SAXS that are strongly model-dependent. Nevertheless, it only provides local information and is therefore prone to give higher uncertainty. The SEM measures the CD at a different height than the other techniques used in this study but enables the

validation of the OCD thanks to its 0.994 correlation with our current OCD model. This highlights the importance of combining several measurements to extract the most information.

Finally, we demonstrated that the difference between the CD extracted by SAXS and OCD is model dependent and requires the development of similar models to enable a good comparison. The models for both techniques can be improved, and the SAXS rounded trapezoid model is a promising research direction, requiring further investigation.

SAXS raw data processing can be improved, specifically intensities interpolation, peaks positions fitting, background noise suppression merit special attention. A better quantification of the technique's uncertainty is necessary to improve inter-techniques comparison and be able to use it as a reference technique.

ACKNOWLEDGEMENTS

This work is funded by the MADEin4 project. MADEin4 has received funding from the Electronic Component Systems for European Leadership Joint Undertaking under grant agreement No 826589. This Joint Undertaking receives support from the European Unions Horizon 2020 research and innovation program and Netherlands, France, Italy, Belgium, Germany, Austria, Hungary and Israel.

This research used the Soft Matter Interfaces Beamline (SMI, Beamline 12-ID) of the National Synchrotron Light Source II, a U.S. Department of Energy (DOE) Office of Science User Facility operated for the DOE Office of Science by Brookhaven National Laboratory under Contract No. DE-SC001270.

We thank Karen Dabertrand and Romain Bon for their help on TEM characterizations, and Olivier Dubreuil for his assistance on OCD modelling and data comprehension.

REFERENCES

[1] 'International Roadmap for Devices and Systems 2021 Edition', IEEE International Roadmap for Devices and Systems TM, Feb. 2021. [Online]. Available: https://irds.ieee.org/editions/2021

[2] B. Bunday, T. A. Germer, V. Vartanian, A. Cordes, A. Cepler, and C. Settens, 'Gaps analysis for CD metrology beyond the 22nm node', presented at the SPIE Advanced Lithography, San Jose, California, USA, Apr. 2013, p. 86813B. doi: 10.1117/12.2012472.

[3] N. G. Orji *et al.*, 'Metrology for the next generation of semiconductor devices', *Nat. Electron.*, vol. 1, no. 10, pp. 532–547, Oct. 2018, doi: 10.1038/s41928-018-0150-9.

[4] J. Reche, 'Nouvelle méthodologie hybride pour la mesure de rugosités sub-nanométriques', Micro et nanotechnologies/Microélectronique, Université Grenoble Alpes, 2019. [Online]. Available: https://tel.archives-ouvertes.fr/tel-02520554v2. NNT: 2019GREAT050

[5] Q. Wang, H. Chen, and S. Hu, 'Verified Optical Scatterometry Model for Line-Space and Metal-Gate Structures', in *2021 International Workshop on Advanced Patterning Solutions (IWAPS)*, Foshan, China, Dec. 2021, pp. 1–4. doi: 10.1109/IWAPS54037.2021.9671253.

[6] D. Dixit *et al.*, 'Characterization of Overlay and Tilt in Advanced Technology Nodes using Scatterometry', in *2019 30th Annual SEMI Advanced Semiconductor Manufacturing Conference (ASMC)*, Saratoga Springs, NY, USA, May 2019, pp. 1–7. doi: 10.1109/ASMC.2019.8791810.

[7] M. H. Madsen and P.-E. Hansen, 'Scatterometry—fast and robust measurements of nano-textured surfaces', *Surf. Topogr. Metrol. Prop.*, vol. 4, no. 2, p. 023003, Apr. 2016, doi: 10.1088/2051-672X/4/2/023003.

[8] P. C. Logofătu, J. R. Mcneil, A. Sima, B. Ioniţă, F. Garoi, and D. Apostol, 'The characterization of gratings using optical scatterometer'.

[9] A. Gunay-Demirkol *et al.*, 'Innovative scatterometry approach for self-aligned quadruple patterning (SAQP) process control', presented at the SPIE Advanced Lithography, San Jose, California, United States, Mar. 2016, p. 977807. doi: 10.1117/12.2220287.

[10] R. L. Jones *et al.*, 'Small angle x-ray scattering for sub-100 nm pattern characterization', *Appl. Phys. Lett.*, vol. 83, no. 19, pp. 4059–4061, Nov. 2003, doi: 10.1063/1.1622793.

[11] T. Hu *et al.*, 'Small angle x-ray scattering metrology for sidewall angle and cross section of nanometer scale line gratings', *J. Appl. Phys.*, vol. 96, no. 4, pp. 1983–1987, Aug. 2004, doi: 10.1063/1.1773376.

[12] G. Freychet *et al.*, 'Estimation of Line Cross Sections Using Critical-Dimension Grazing-Incidence Small-Angle X-Ray Scattering', *Phys. Rev. Appl.*, vol. 12, no. 4, p. 044026, Oct. 2019, doi: 10.1103/PhysRevApplied.12.044026.

[13] D. F. Sunday, S. List, J. S. Chawla, and R. J. Kline, 'Determining the shape and periodicity of nanostructures using small-angle X-ray scattering', *J. Appl. Crystallogr.*, vol. 48, no. 5, pp. 1355–1363, Oct. 2015, doi: 10.1107/S1600576715013369.

[14] D. F. Sunday *et al.*, 'X-ray characterization of contact holes for block copolymer lithography', 2020.

[15] R. J. Kline, D. F. Sunday, D. Windover, and B. D. Bunday, 'X-ray scattering critical dimensional metrology using a compact x-ray source for next generation semiconductor devices', *J. MicroNanolithography MEMS MOEMS*, vol. 16, no. 1, p. 014001, Feb. 2017, doi: 10.1117/1.JMM.16.1.014001.

[16] J. Reche, Y. Blancquaert, G. Freychet, P. Gergaud, and M. Besacier, 'Dimensional Control of Line Gratings by Small Angle X-Ray Scattering: Shape and Roughness Extraction', in *2020 31st Annual SEMI Advanced Semiconductor Manufacturing Conference (ASMC)*, Saratoga Springs, NY, USA, Aug. 2020, pp. 1–6. doi: 10.1109/ASMC49169.2020.9185351.

[17] J. Reche, P. Gergaud, Y. Blancquaert, M. Besacier, and G. Freychet, 'Shape and Roughness Extraction of Line Gratings by Small Angle X-Ray Scattering: Statistics and Simulations', *IEEE Trans. Semicond. Manuf.*, vol. 35, no. 3, pp. 425–431, Aug. 2022, doi: 10.1109/TSM.2022.3176026.

[18] G. Freychet, 'Analyses morphologiques et dimensionnelles de nanostructures organisées par diffusion centrale des rayons X', Micro et nanotechnologies/Microélectronique, Université Grenoble Alpes. [Online]. Available: https://tel.archives-ouvertes.fr/tel-01612242. NNT: 2016GREAY076

[19] M. Zhernenkov, N. Canestrari, O. Chubar, and E. DiMasi, 'Soft matter interfaces beamline at NSLS-II: geometrical ray-tracing vs. wavefront propagation simulations', presented at the SPIE Optical Engineering + Applications, San Diego, California, United States, Sep. 2014, p. 92090G. doi: 10.1117/12.2060889.